Hindawi
International Journal of Energy Research
Volume 2024, Article ID 5538071, 16 pages
https://doi.org/10.1155/2024/5538071

Research Article

Effects of Fuel Flow and Airflow Swirl on Thermal Performance of a Miniature-Scale Combustor for Direct Energy Conversion Systems

Soroush Sheykhbaglou,[1] **Amirreza Ghahremani**,[1] **Sadegh Tabejamaat**,[1] **and Mario Sánchez-Sanz**[2]

[1]*School of Mechanical, Aerospace, and Maritime Engineering, Amirkabir University of Technology (Tehran Polytechnic), No. 350, Hafez Ave, Tehran, Iran*
[2]*Departamento de Ingeniería Térmica y de Fluidos, Universidad Carlos III de Madrid, Leganés 28911, Spain*

Correspondence should be addressed to Amirreza Ghahremani; a_ghahremani@aut.ac.ir

Received 10 July 2023; Revised 12 January 2024; Accepted 18 March 2024; Published 4 April 2024

Academic Editor: Vinayak Parale

Micropower generation and micropropulsion are two emerging fields where micro- and miniature-scale combustors are anticipated to play a significant role. Today, there is a growing interest in combustion-based direct energy conversion modules such as thermoelectric and thermophotovoltaic micropower generators. In this study, the effects of swirl addition to fuel flow and airflow on combustor operational envelope, flame blowout limit, combustion efficiency, exhaust gas temperature, mean outer wall temperature, emitter efficiency, and normalized temperature standard deviation of a miniature-scale (mesoscale) combustor are studied under various equivalence ratios. The findings demonstrate that swirling flows improve the flame blowout limit and operational envelope of the combustor; however, this improvement is more significant for airflow swirl. Besides simultaneous swirling flows of fuel and air result in the highest blowout limit. Additionally, it has been shown that swirl addition improves combustion efficiency and causes a significant amount of heat to be generated, which raises the temperature of the exhaust gas, the mean outer wall temperature, and the emitter efficiency. Furthermore, mean outer wall temperature and emitter efficiency have the highest values for simultaneous swirling flows of fuel and air. It is also observed that increasing the fuel flow swirl number generally lessens the normalized temperature standard deviation (NTSD) and consequently improves the combustor wall temperature uniformity, while for the airflow swirl case, a swirler with 30° vane angle for airstream has a lower NTSD than a 45° vane angle swirler. The results obtained in this study provide useful information for designing a combustion-based direct energy conversion module.

1. Introduction

At present, with the increasing demand of microdevices, the need for high-density power sources for long operation periods has noticeably increased. The significant energy density of hydrocarbon fuels, short recharge periods, and advances in the miniaturization of devices have drawn attention to combustion-based micropower generators [1–3]. Typical hydrocarbon fuels have energy densities approximately 50 to 100 times higher than modern batteries. Even, with taking into account the conversion efficiency of combustion-based power systems, they are considered as a viable alternative to batteries for portable power generation. Hence, studying microscale combustion is of great importance in micropower generation and chemical microthrusters for small spacecrafts which can be utilized in orbit change and attitude control [4–6].

One approach to define a "microscale" combustion is based on the physical dimensions of the combustor: if the characteristic physical length is less than 1 or 2 mm, the combustion is called "microcombustion," and if the above-mentioned length is of the order of a few millimeters, the combustion is called "mesoscale combustion" [7]. As the

combustor size is decreased, flame extinction due to thermal and radical quenching is inevitable. The former is due to an increase in the surface-to-volume ratio and large surface heat loss, and the latter results from the absorption and recombination of excessive chain branching radicals [7]. Large heat loss from micro- or mesoscale combustors is favorable for direct energy conversion modules such as thermoelectric (TE) and thermophotovoltaic (TPV) generators. Several strategies have been offered and employed for flame stabilization in micro- and mesoscale combustion such as catalytic combustion [8–10], excess enthalpy concept [11–13], and vortex flows [14–17]. Lei et al. [18] developed a microcombustor taking advantage of the excess enthalpy concept for micropower generation using a TPV cell. They reached a maximum overall chemical-electrical conversion efficiency of 3.15% in a combustor with a 1 mm inner diameter. They found out that a combustor with heat recirculation has a higher flammability limit than one without heat recirculation. Gan et al. [19] developed a mesoscale combustor with electrospray which can be coupled with direct energy systems for power generation. Thermal efficiencies ranging from 22.0 to 48.0% were obtained in their work. Hosseini et al. [15] studied a mesoscale vortex combustor with and without thermal recuperation. Thermal recuperation resulted in higher emitter and thermal efficiency. Shimokuri et al. [20] developed a TE combustion-based power generation system using vortex flow. Maximum electrical output power of 8.1 W was reached at the thermal input power of 355 W with 2.4% conversion efficiency. Yang et al. [21] studied the thermal performance of a microswirl combustor in premixed and nonpremixed modes comparatively. Their results showed that the premixed mode has better thermal performance at small equivalence ratios and leads to better wall temperature uniformity at high hydrogen mass flow rates. Another type of micropower generation device is combustion-based indirect energy conversion modules which involve complex moving components and frictional losses. MEMS-based silicon gas-turbine engines were built at MIT with an overall size of 2.1 cm × 2.1 cm × 0.38 cm [22, 23]. The utilized fuel was hydrogen, and the output electrical power was ranging between 10 and 50 W. A MEMS-based microrotary engine with a rotor size of 10 mm was developed at the US Berkeley Combustion Lab [24]. A hydrogen/air mixture was used, and an electrical power of 3.7 W was obtained at 9000 rpm. A microscale rotating free piston engine was developed at the University of Michigan which was capable of operating in a four-stroke Otto cycle and producing an electrical power of 20 W [25]. The fuel was butane. and the overall conversion efficiency was 14%. This micropropulsion engine is one of the other promising applications of microcombustion. The aim of the micropropulsion and microthrusters is to meet as the main propulsion and attitude control of a microspacecraft. Wu et al. [14] tested micro- and mesoscale vortex combustors for gaseous flame stabilization which can be utilized in micropower generation and micropropulsion systems. Various fuels were studied, and it was found out that flame stabilization in small combustors requires the enrichment of oxygen. A maximum chemical efficiency of 97% and 85% were obtained for hydrogen/air mixtures and methane/oxygen/air, respectively. Wu and Lin [26] developed a bipropellant microthruster. The dimensions of the thruster chamber were 5.22 mm × 1.6 mm × 1.19 mm. The output thrust was between 0.2 mN and 1.97 mN and was linearly proportional to the total mass flow rate.

Although vortex and swirl combustion have been proposed and utilized in micro- and mesoscale combustion, using double annulus axial flat vane swirlers to fuel flow and airflow to stabilize methane/air flames for potential uses in micropower generation has not been studied and compared as far as authors' knowledge. Hence, the present work focuses on the effects of fuel flow and airflow swirl on the stability and thermal performance of a miniature-scale (mesoscale) combustor for possible use in direct energy conversion systems such as TE and TPV generators.

2. Experimental Setup and Flow Delivery System

The experimental setup and swirl burner are shown in Figures 1(a) and 1(b), respectively. The setup consists of air and fuel supply systems, a data acquisition system for exhaust gas and wall temperature distribution measurement including ADAM 4018+ and ADAM 4520, six 0.5 mm K-type thermocouples, a flue gas analyzer, and a digital camera. The methane and air are supplied to the burner from an air compressor and high-pressure cylinder, respectively, which are equipped with pressure reduction valves and pressure gauges. The mass flow rates of methane and air are regulated precisely by Kobold DMS-5 and AZBIL MPC0020 mass flow controllers with the accuracy of ±1% full scale, respectively. In order to measure postcombustion emission, the combustor is placed inside a steel-made duct with a visualization window for imaging. Six temperature-measuring holes, five for the temperature distribution of the combustor outer wall and one for exhaust gas measurement, are drilled along the duct. Flue gas concentrations are measured using a Testo 350-XL flue gas analyzer. The measuring ranges and accuracies of this analyzer are presented in Table 1. The flame images are captured taking advantage of a Canon PowerShot G16 digital camera with an exposure time of 1/30 s. Ambient conditions were obtained using Lutron PHB-318, and values for pressure, temperature, and humidity were 88270 ± 15 Pa, 23.9 ± 0.8°C, and 28.5 ± 3%, respectively. In order to study the effects of fuel flow and airflow swirl, five double annulus axial flat vane swirlers were built by the selective laser melting (SLM) process. A quartz mesoscale combustor was used in this study. Its length, inner diameter, and thickness are 50 mm, 8.8 mm, and 1.6 mm, respectively. The flow swirl strength is characterized by a nondimensional swirl number which is calculated as follows [25]:

$$S_n = \frac{2}{3}\frac{1-(D_h/D_{sw})^3}{1-(D_h/D_{sw})^2}\tan\theta, \quad (1)$$

where D_h, D_{sw}, and θ are the swirler hub diameter, swirler tip diameter, and vane angle, respectively. Table 2 presents the specifications of the constructed swirlers.

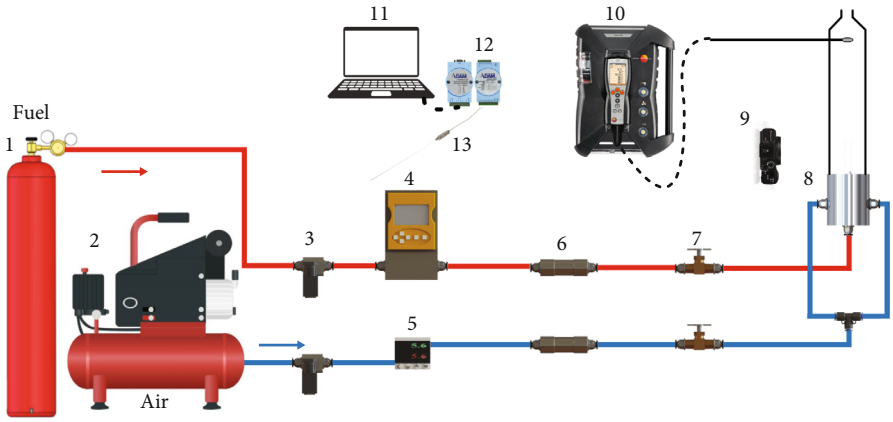

(1) High pressure methane cylinder with pressure reduction valve and gauge
(2) Air compressor with air dryer and pressure reduction valve and guage
(3) Solenoid valve
(4) Fuel mass flow controller
(5) Air mass flow controller
(6) Check valve
(7) Needle valve
(8) Swirl burner and meso-scale combustor
(9) Digital camera
(10) Flue gas analyzer and its probe
(11) Laptop
(12) ADAM 4018+ and ADAM 4520
(13) 6 flexible K-type flexible thermocouples

Air
Fuel

(a)

(1) Air inlets
(2) Fuel inlet
(3) Plenum
(4) Axial swirler
(5) Quartz combustor

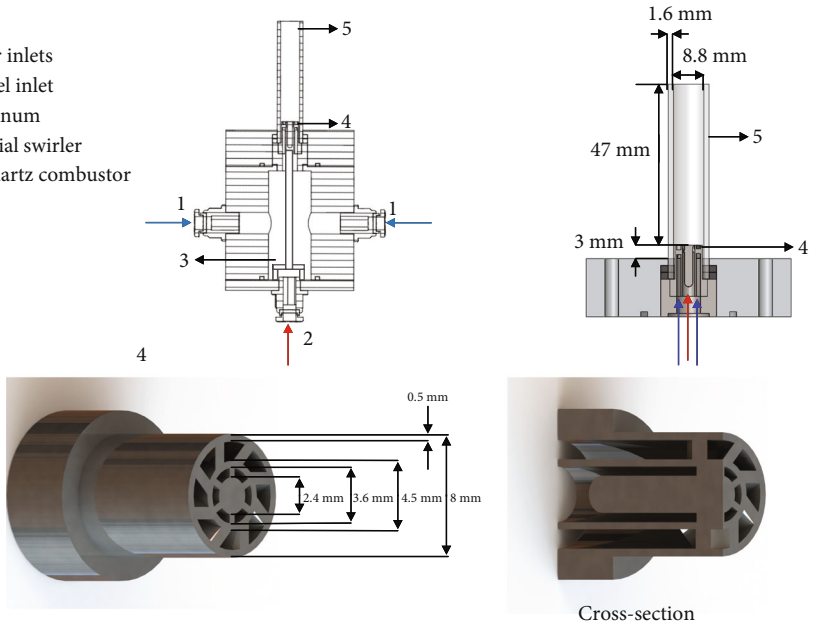

Fuel
Air

(b)

Figure 1: Continued.

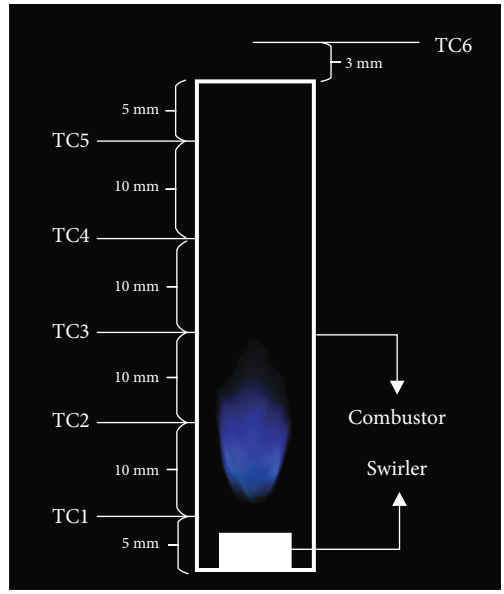

(c)

Figure 1: (a) Experimental setup and flow delivery system. (b) Swirl burner, miniature-scale combustor, and axial swirler geometry. (c) K-type thermocouples.

Table 1: Measuring ranges and accuracies using Testo 350-XL flue gas analyzer.

Parameters	Measuring range	Accuracy	Resolution
O_2	0…25 vol. %	±0.2 vol. %	0.01 vol. %
CO, H_2-comp	0…10000 ppm	±10 ppm (0…99 ppm) ±5% of reading (100…2000 ppm) ±10% of reading (2001…10000 ppm)	1 ppm
CO_{low}, H_2-comp	0…500 ppm	±2 ppm (0…39.9 ppm) ±5% of reading (40…500 ppm)	0.1 ppm
CO_2 (IR)	0…50 vol. %	**±0.3 vol**.% + **1**% of reading (0…25 vol. %) **±0.5 vol**.% + **1.5**% of reading (25.1…50 vol. %)	0.01 vol. % 0.1 vol. %

Table 2: Specifications of studied swirlers.

		Inner annulus		Outer annulus	
Swirler no.	Name	Vane angle (°)	S_n (-)	Vane angle (°)	S_n (-)
1	F0O0	0	0	0	0
2	F30O0	30	0.49	0	0
3	F45O0	45	0.84	0	0
4	F0O30	0	0	30	0.48
5	F0O45	0	0	45	0.83
No. of vanes		6		8	
Vane thickness (mm)		0.45		0.80	
Hub diameter (mm)		2.4		4.5	
Tip diameter (mm)		3.6		7	

3. Results and Discussion

In this section, the effects of fuel flow and airflow swirl on the combustor operational envelope (stability map), flame characteristics, and emission and thermal performances of the mesoscale combustor are studied under various equivalence ratios. The mentioned equivalence ratio is the global equivalence ratio which is defined as $\Phi = (\dot{m}_{air}/\dot{m}_{fuel})_{stoic}/(\dot{m}_{air}/\dot{m}_{fuel})$. The numerator of this ratio is the stoichiometric air-to-fuel ratio (which is 17.1 for

methane and air), and the denominator is the ratio of supplied mass flow rates of air and fuel to the combustor.

3.1. Fuel/Oxidizer Swirl

3.1.1. Flame Characteristics and Combustor Operational Envelope. Practical combustion systems often include swirling flows because of the well-known role that swirl plays in flame stability [27, 28]. According to [29], turbulent burning velocity is enhanced by using a swirl, and the recirculation zone induced by swirling flows acts as a heat source and entrains hot products inside fresh reactants. Hence, the fuel flow and airflow swirl on the stability map of the combustor are investigated. The process for determining the operational envelope of the combustor for each swirler is as follows: First, a specified fuel flow rate is supplied, and a stable diffusion flame is formed at the combustor rim; next, the air is fed, and its flow rate is raised by 0.1 slpm. The airflow rate at which the flame moves inside the combustor is defined as the lower limit of the operational envelope for the set fuel flow rate. The airflow rate is increased until the flame inside the combustor extinguishes (blows out) owing to low residence time. The airflow rate at which the flame blows out is the operational envelope's upper limit (or blowout). Hence, the flame can sustain inside the mesoscale combustor between these two limits. These steps are repeated for fuel flow rates varying from 0.050 slpm to 0.500 slpm, and the combustor operational envelope is obtained for each swirler. The procedure is repeated three times for each fuel flow rate, and the average values for lower and upper limits are reported in this study. As presented in Table 1, five axial flat vane swirlers are utilized to study the flow swirl. Each swirler is designated a name which corresponds to its fuel or airflow (oxidizer) vane angle. For example, F0O30 indicates a swirler in which the fuel is in jet form and the oxidizer (air) is passed through vanes of the angle of 30°. Figures 2(a) and 2(b) illustrate the effects of fuel flow and airflow swirl on the combustor operational envelope, respectively. The observations are as follows:

(i) Both lower and upper limits increase with an increment in the fuel flow rate

(ii) Nonswirling flames (F0O0) and flames with fuel flow swirl configurations cannot sustain inside the combustor for fuel flow rates greater than 0.150 slpm

(iii) Adding a swirl to fuel or airflow rate causes the flames to move inside the combustor at lower airflow rates compared with nonswirling flames due to the well-known effects of swirling flows in fuel/air mixing. Although adding a swirl to fuel flow enhances the operational envelope of the combustor, a coaxial airflow swirl has a more noticeable effect. F30O0 and F45O0 configurations enhance the operational envelope by approximately 11% and 30%, while the enhancement for F0O30 and F0O45 is 798% and 862%, respectively, when compared with nonswirling flames

(iv) Stable flames inside the combustor are formed mostly in fuel-lean conditions

(v) When the methane flow rate is lower than 0.200 slpm, the flame resistance against extinction is better for F0O30 when compared with F0O45, although for fuel flow rates equal and greater than 0.200 slpm, F0O45 presents better performance in the blowout limit. The latter is because of the well-known effect of swirling flows in flame stabilization leading to better mixing of fuel and oxidizer due to enhancement of the turbulent burning velocity, acting as a heat source, increasing the residence time, and perquisite role of recirculation zone induced by swirling flows in flame anchoring [27–30], while in the former, the swirl effect may be negligible and less due to lower airflow rates for blowout limit

(vi) As shown in Figure 2(b), in a narrow part of the operational envelope of F0O45 shown in cyan color and is near to blowout limit, the flame changes between type A and type B. As the airflow rate increases, the frequency of this occurrence increases, too. Then, the flame takes the type B form and then blows out with an additional airflow increment

Figure 3 represents flame images as a function of equivalence ratio where the methane flow rate is fixed at 0.150 slpm. It is observed that the swirl strength of air has a noticeable influence on flame appearance and shape. It is also observed that F0O30 reveals bowl-shaped flames. Besides, flame lift-off height and length decrease with a decrease in the equivalence ratio (increase in the airflow rate) where the fuel flow rate is fixed. Indeed, the lift-off height of F0O0, F30O0, and F45O0 flames are more sensitive to equivalence ratio when compared with airflow swirl modes. It is observed that some reddish and yellowish zones downstream of the primary zone at equivalence ratios near 1, which is an indication of soot formation and represents that some of the fuel is not mixed thoroughly into the air stream, and there are localized rich regions.

The effects of the fuel flow rate on nondimensional flame lift-off height and length where the airflow rate is fixed at 2.4 slpm are presented in Figure 4. The flame lift-off height (LO) and length (L) are determined using the same image processing techniques as those used in [31–33]. LO is defined as the length between the flame base and the swirler exit plane, and L is defined as the length between the flame tip and base. This is done by applying a 50% intermittency distribution to a series of 100 images for each operating condition in order to generate the flame probability distribution. It is shown that for all cases, increasing the fuel flow rate at a given airflow increases the flame lift-off height and length almost linearly. This behavior is due to decreasing the flow residence time by increasing the fuel flow rate. As the fuel flow rate is increased, the fuel is not entrained and mixed with the air in an effective manner, and the methane and air mix

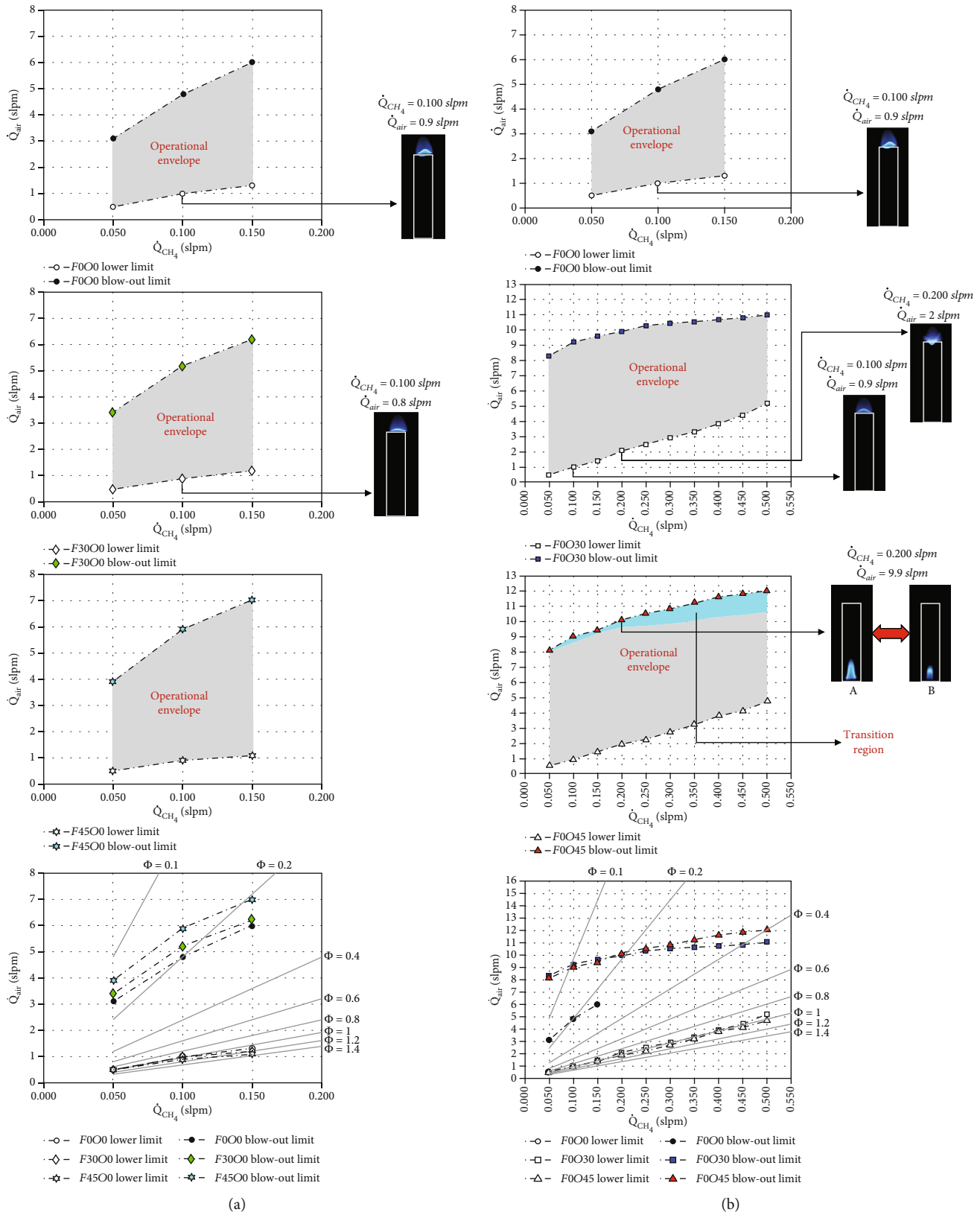

Figure 2: Effects of (a) fuel flow swirl and (b) airflow swirl on the combustor operational envelope.

over a longer distance, which subsequently leads to an increase in LO and L. Besides, according to the curve-fitting, lift-off of flames related to the F0O30 swirler exhibits the least sensitivity compared to the flames of the other studied swirlers (category 1: F0O0, F30O0, and F45O0; category 2: F0O0, F0O30, and F0O45). It is also revealed that the flame

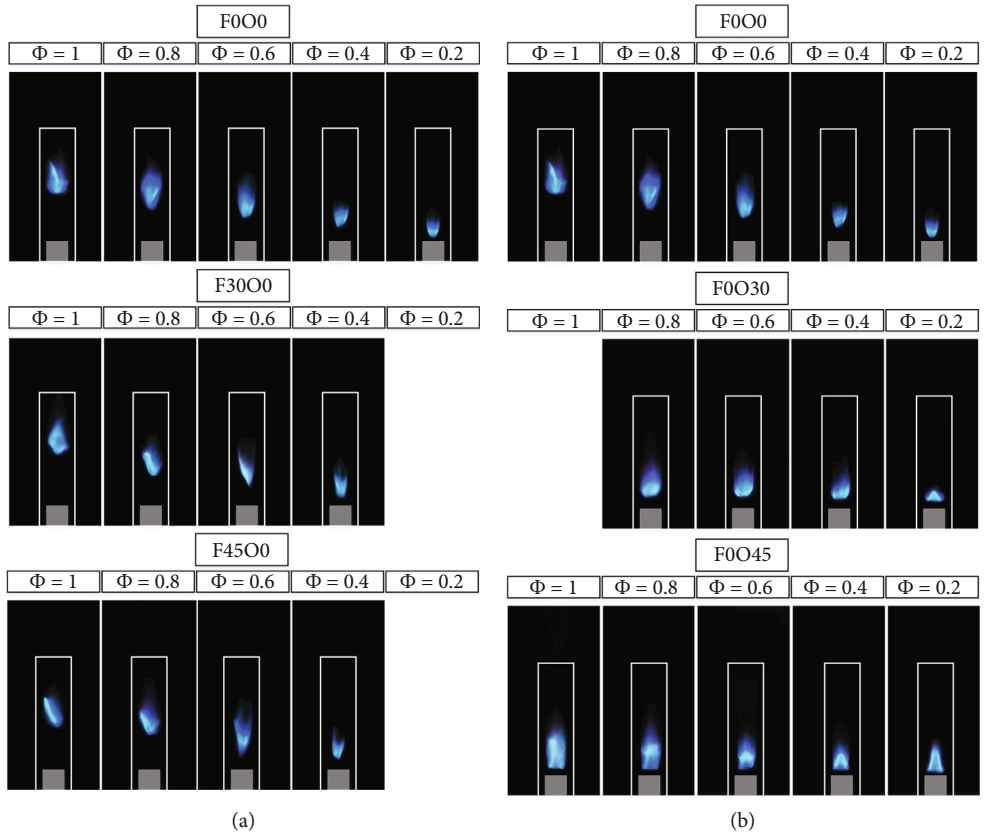

Figure 3: Effects of equivalence ratio on flame appearance for (a) fuel flow swirl and (b) airflow swirl at the fixed fuel flow rate of 0.150 slpm.

length increases at almost the same rate as an increment in the fuel flow rate for the flames of the second category.

3.1.2. Emission and Thermal Performance. Large values of carbon monoxide (CO) in the flue gas are an indication of incomplete combustion which results from imperfect mixing of fuel and air and short residence time. Complete combustion (low values of CO) is accompanied by a significant amount of heat [34]. CO oxidation is feasible through the two following routes [35]:

(1) Wet route

$$\mathrm{CO + OH \longrightarrow CO_2 + H} \quad (2)$$

In the wet route, OH radical plays a significant role in CO oxidation to CO_2. This radical is formed mainly through the following chain branching step which is active for temperatures above 1100 K.

$$\mathrm{H + O_2 \longrightarrow OH + O} \quad (3)$$

(2) Dry route

$$\mathrm{CO + O_2 \longrightarrow CO_2 + O} \quad (4)$$

In this route, oxygen (O_2) availability is of great importance in carbon monoxide oxidation, so in the fuel-rich zones of the combustion, this route loses its effect in carbon monoxide oxidation. Similar to the previous route, the dry route is also active for temperatures above 1100 K.

Figure 5 is an illustration of the CO concentration versus the methane/air equivalence ratio where the methane flow rate is fixed at 0.150 slpm under fuel flow and airflow swirl. Increasing the equivalence ratio at a constant fuel flow rate means a decrease in the airflow rate. It is observed that the CO emission has a U-shaped dependence on the equivalence ratio for all swirlers. This trend can be explained by dividing the curves into three sections:

(i) Section I: $0.2 \leq \Phi < 0.5$

In this section, large values of CO result from high airflow rate and consequently short residence time, insufficient mixing of fuel and air, and low combustion temperature which is discussed later that suppresses both routes of CO oxidation.

(ii) Section II: $0.5 \leq \Phi < 0.8$

In this section, the lowest values of CO and the most complete combustion occur which is due to high combustion temperature, a decrease in the airflow rate, and sufficient residence time for fuel and air for reaction. This section is accompanied by a large amount of heat due to

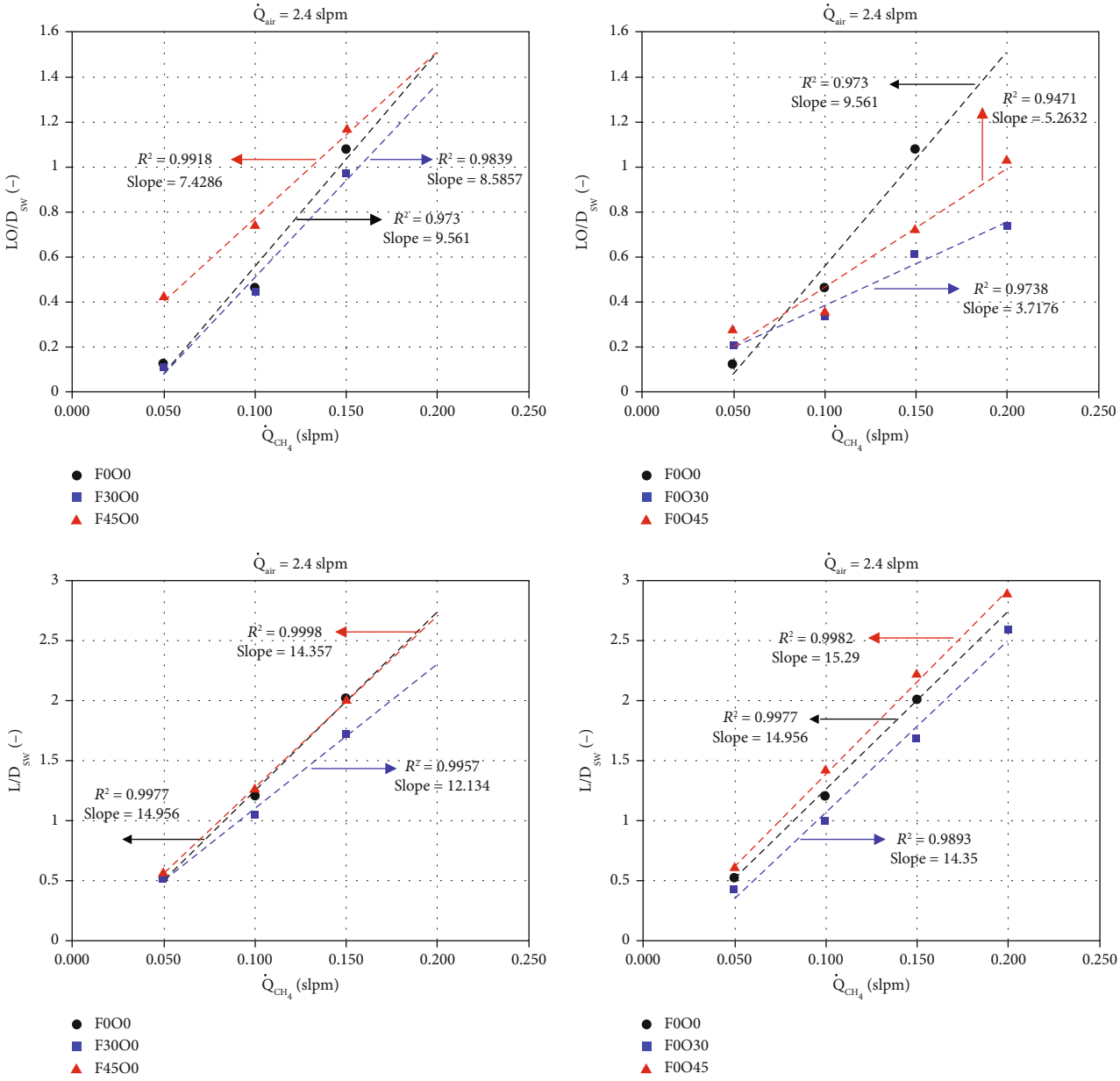

Figure 4: Effects of fuel flow rate on flame lift-off height and length of various swirlers at the fixed airflow rate of 2.4 slpm.

combustion completeness and better efficiency. The minimum CO takes place at the equivalence ratio of 0.7.

(iii) Section III: $\Phi \geq 0.8$

In this part, the airflow rate is low and O_2 availability plays the most significant role in CO oxidations, although the combustion temperature does not differ noticeably from the previous section. Low amounts of O_2 can deactivate both the dry route and wet route by suppressing OH radical production.

It is also shown that adding swirl to fuel flow and airflow lowers the CO emission in the fuel gas which can be attributed to the favorable effect of swirl on flow residence time and methane/air mixing. So, it can be concluded that fuel flow and airflow swirl lead to complete combustion and a large amount of heat produced.

According to [36], the ratio of CO_2/CO on the mass basis is an indication of hydrocarbon conversion and combustion efficiency. Hence, this parameter is studied to compare the non-swirling and swirling flames on combustion efficiency. Figure 6 shows the ratio of CO_2/CO on the mass basis as a function of the equivalence ratio at the fuel flow rate of 0.150 slpm. It is observed that CO and the ratio of CO_2/CO are related to each other in an inverse manner, and the second section of the CO curves as discussed earlier has the highest combustion efficiency. Furthermore, it is obvious that adding a swirl rises this ratio and consequently improves combustion efficiency.

Figure 7 illustrates the effects of the equivalence ratio on the exhaust gas temperature (T_{exh}) where the methane flow rate is fixed at 0.150 slpm. The TC6 K-type thermocouple which is located 3 mm above the combustor exit plane is used to measure the temperature of the exhaust gas (Figure 1(c)). It

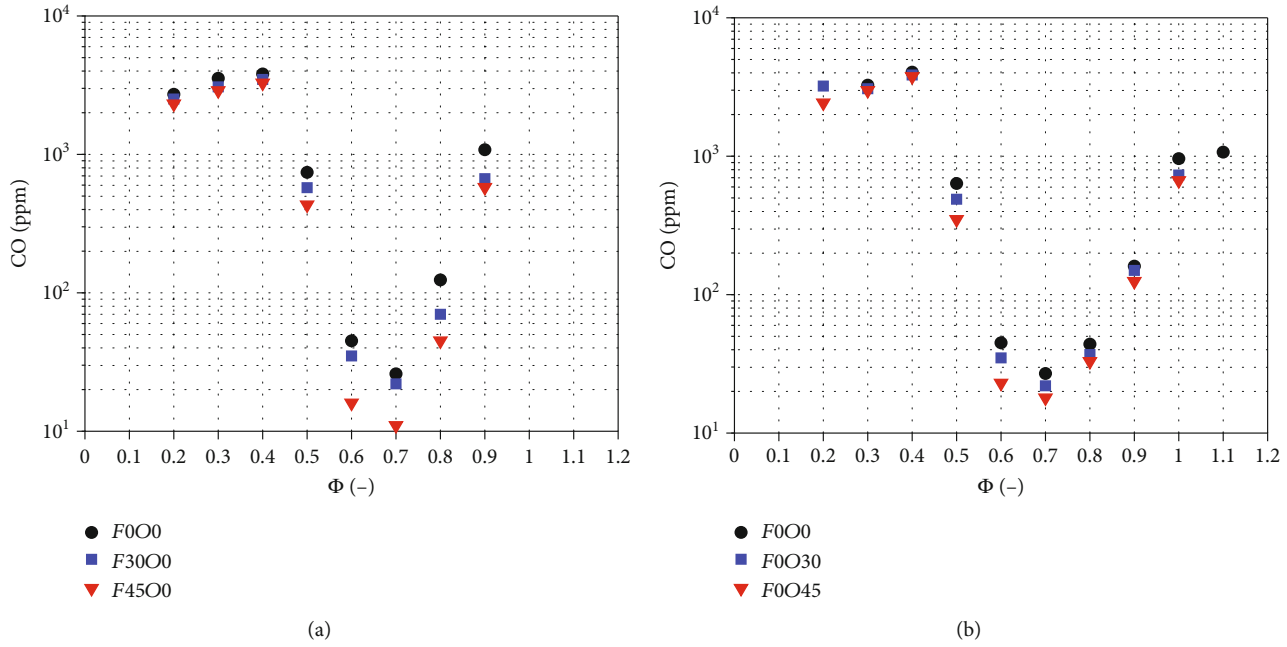

Figure 5: Effects of (a) fuel flow swirl and (b) airflow swirl on CO concentration as a function of equivalence ratio at the fuel flow rate of 0.150 slpm.

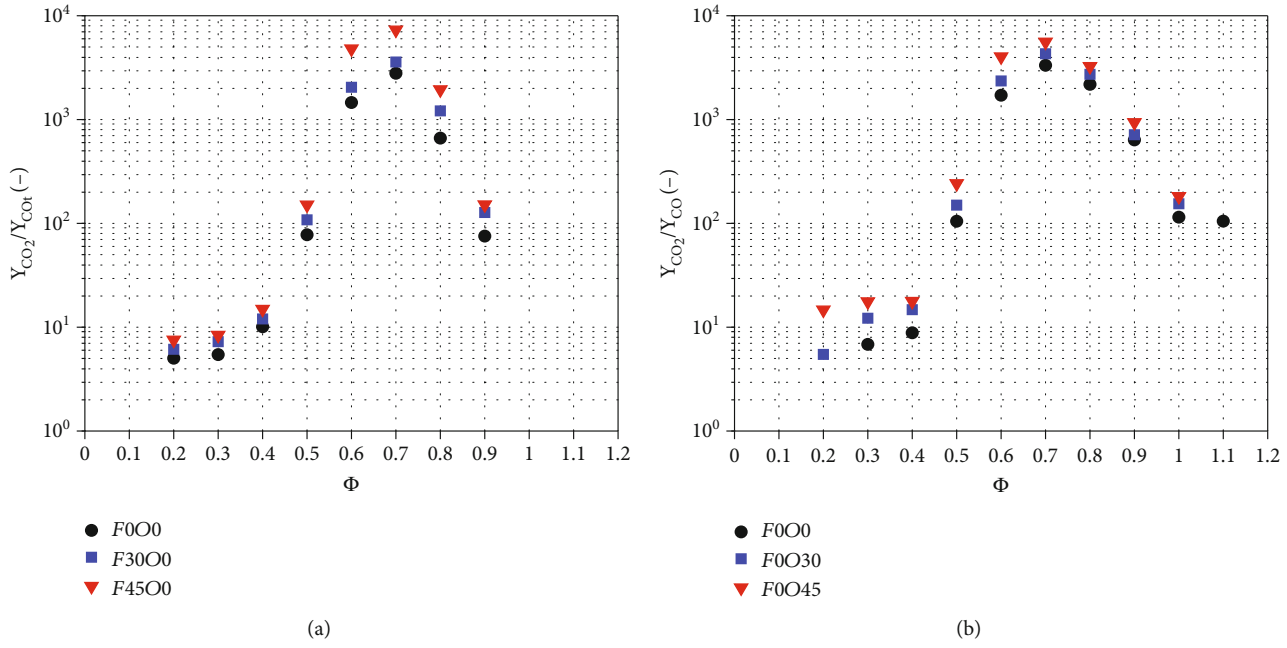

Figure 6: Effects of (a) fuel flow swirl and (b) airflow swirl on the ratio of CO_2/CO on the mass basis as a function of equivalence ratio at the fuel flow rate of 0.150 slpm.

is observed that T_{exh} has an increasing-decreasing trend with an increment in the equivalence ratio. This trend can be explained in Figure 6 in which the ratio of CO_2/CO versus the equivalence ratio shows a similar trend. As stated earlier, high values of this ratio indicate high combustion efficiency and consequently high combustion temperature. The exhaust gas temperature can be a good representation of the combustion temperature. It is shown that the temperature of the exhaust gas is low at low equivalence ratios, so it can be concluded that the combustion efficiency is low, too. Hence, due to low combustion temperature, CO oxidation through wet and dry routes, which are active at temperature above 1100 K, is suppressed (Figure 5). It is observed that adding a swirl increases the exhaust gas temperature due to its positive effect on combustion efficiency.

The significant energy density of hydrocarbon fuels and large heat loss in the forms of radiation and convection from micro- and mesoscale combustors make small-scale

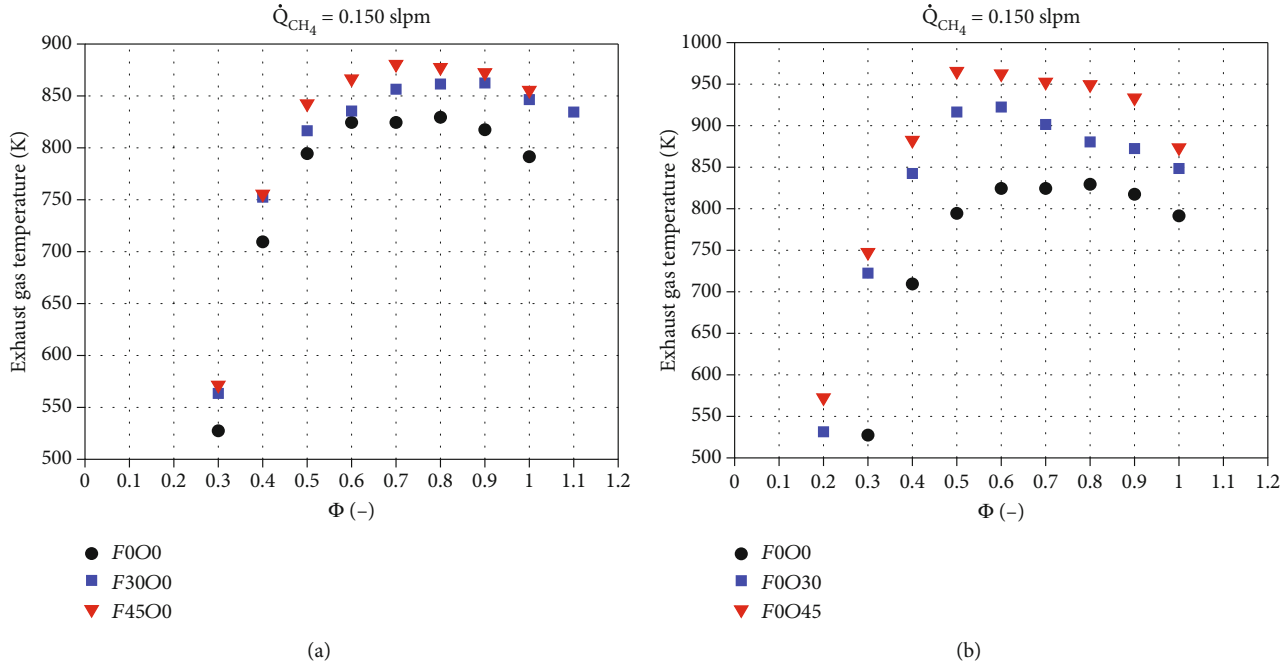

Figure 7: Effects of (a) fuel flow swirl and (b) airflow swirl on the exhaust gas temperature as a function of equivalence ratio at the fuel flow rate of 0.150 slpm.

combustion-based direct energy conversion modules such as TE and TPV generators for micropower generation attractive alternatives to batteries. In these modules, the combustor outer wall temperature, its uniformity, and emitter efficiency play the most significant role in micropower generation. So, the focus of this part is on the effects of fuel flow and airflow swirl on combustor mean outer wall temperature, its uniformity which is characterized by normalized temperature standard deviation (NTSD), and emitter efficiency. As depicted in Figure 1(c) schematically, the outer wall temperature distribution is obtained using five K-type thermocouples which are contacted to the outer wall with a thermal paste to ensure better conductivity and heat transfer. The abovementioned parameters are expressed as follows:

$$T_{\text{ave}} = \frac{\sum A_{w,i} T_{w,i}}{\sum A_{w,i}}, \tag{5}$$

$$\dot{Q}_{\text{rad}} = \sum A\varepsilon\delta\left(T_{\text{ave}}^4 - T_{\text{amb}}^4\right), \tag{6}$$

$$\eta = \frac{\dot{Q}_{\text{rad}}}{\dot{m}_{CH_4} \times \text{LHV}_{CH_4}} \times 100\%, \tag{7}$$

$$\text{NTSD} = \frac{\sum A_{w,i} \left| T_{w,i} - T_{\text{ave}} \right|}{T_{\text{ave}} \sum A_{w,i}} \times 100\%, \tag{8}$$

where T_{ave}, $\dot{Q}_{\text{rad}}$, η, and NTSD are mean outer wall temperature, radiation heat loss, emitter (radiation) efficiency, and normalized standard deviation. In Eq. (5), $A_{w,i}$ and $T_{w,i}$ are the area and temperature of the wall of the ith element. In Eq. (6), A, ε, δ, and T_{amb} are combustor outer wall surface area, emissivity of the wall, Stephen Boltzmann constant (5.67×10^{-8} W/(m^2 – K^4)), and ambient temperature. In Eq. (7), $\dot{m}_{CH_4}$ and LHV_{CH_4} are methane mass flow rate and lower heating value. Figure 8 illustrates the effect of fuel flow and airflow swirl on the mean outer wall temperature and emitter efficiency at various methane/air equivalence ratios where the methane flow rate is fixed at 0.150 slpm. It is observed that mean outer wall temperature and emitter efficiency exhibit an increasing-decreasing trend which can be explained by the ratio of CO_2/CO versus the equivalence ratio plots (Figure 6). It is also observed that swirl addition to fuel flow and airflow increases both mean outer wall temperature and emitter efficiency. The former is because of the combustion efficiency enhancement and an increase in the amount of heat released by swirl addition as discussed before and the latter results from Eqs. (7) and (8) in which larger mean outer wall temperature leads to higher emitter efficiency. It is observed that a maximum emitter efficiency of about 7% and 8% are obtained for F45O0 and F0O45 configurations, respectively. Hence, it can be concluded that flows with high swirl numbers are better choices for TPV power generators from the emitter efficiency point of view among these swirlers with only fuel or air swirl.

Figure 9 presents the effects of methane flow rate on mean outer wall temperature and emitter efficiency at the fixed airflow rate of 2.4 slpm. As this figure shows, mean outer wall temperature and emitter efficiency reveal an increasing trend by increasing the fuel flow rate. This trend is due to an increase in the input power by incrementing the fuel flow rate that leads to large heat release. Furthermore, it is observed that increasing the swirl number enhances the mean outer wall temperature and emitter

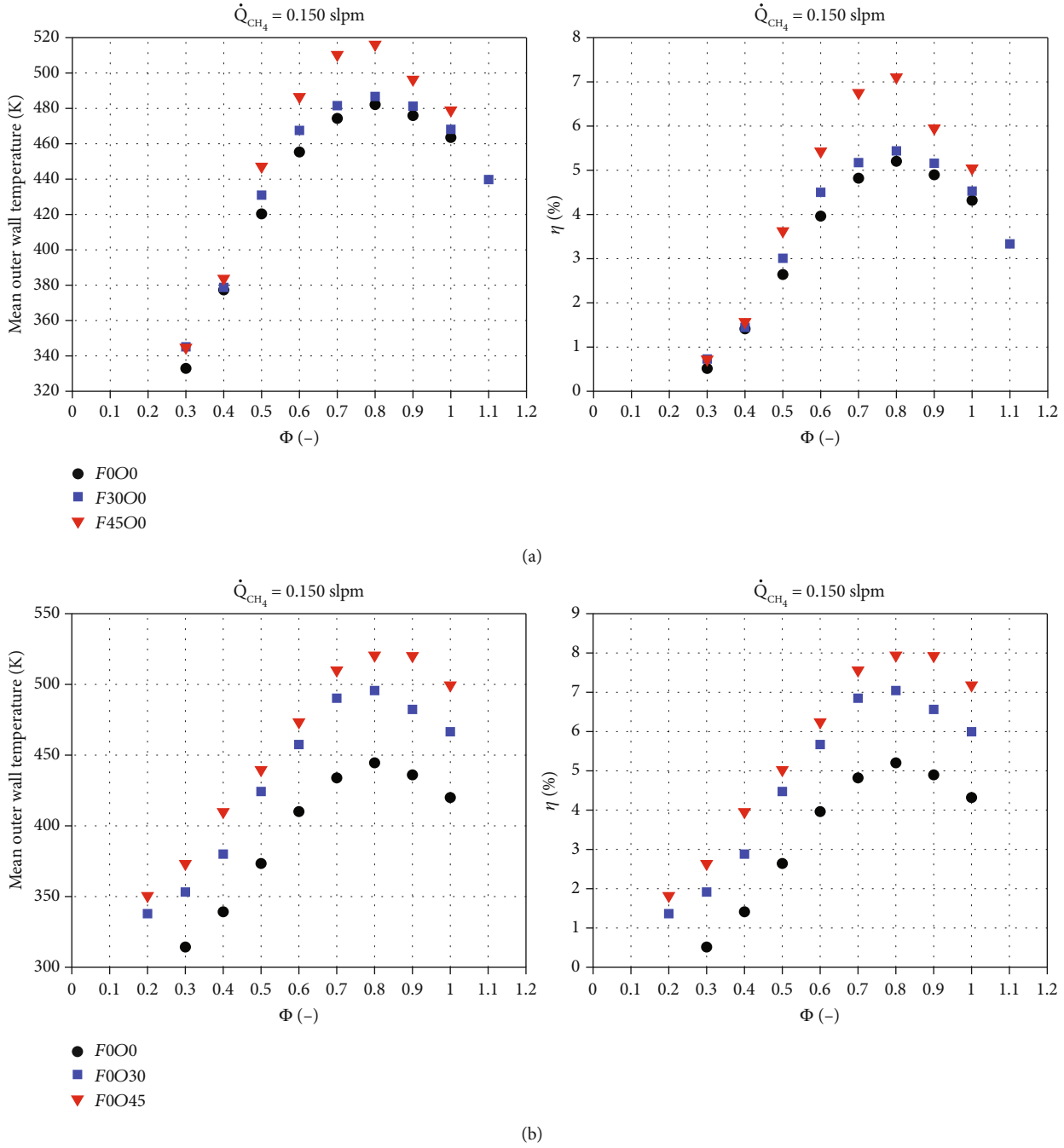

Figure 8: Effects of (a) fuel flow swirl and (b) airflow swirl on the mean outer wall temperature and emitter efficiency as a function of equivalence ratio at the fuel flow rate of 0.150 slpm.

efficiency because of the enhancement of combustion efficiency and the amount of heat released at the same operating conditions (Figure 6). The enhancement of the emitter efficiency when compared with nonswirling flames is presented in Table 3 for three fuel flow rates.

Figure 10 shows the effects of fuel flow, airflow swirl, and equivalence ratio on the normalized temperature standard deviation (NTSD) which is an indication of wall temperature uniformity. It is observed that the obtained NTSD for the studied operating conditions is less than 18%, and the NTSD generally increases with an increment in the equivalence ratio except for the F0O30 configuration which shows an increasing-decreasing-increasing trend. From Figure 10(a), it is also observed that the NTSD of F45O0 is less than that of F30O0, and for $\Phi \geq 0.5$, the F45O0 configuration reveals the lowest values of NTSD among studied configurations in fuel flow swirl mode (F0O0, F30O0, and F45O0). So, it can be concluded that a high fuel flow swirl number is a good choice to get the most uniform wall temperature. The highest value of NTSD among these configurations is

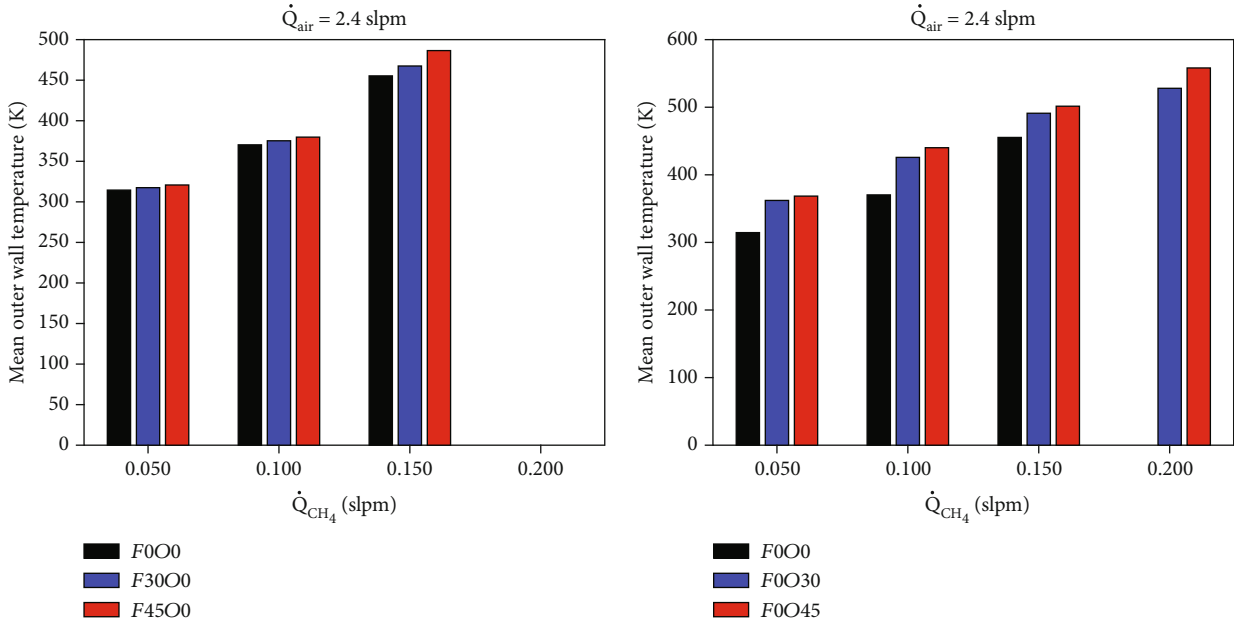

(a)

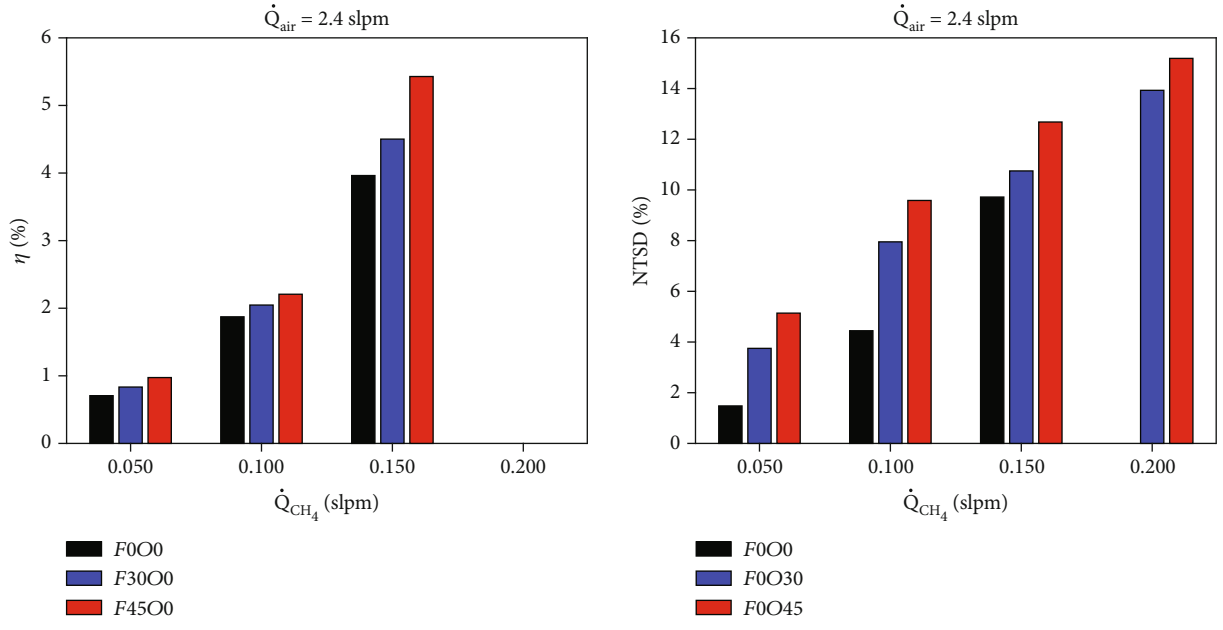

(b)

Figure 9: Effect of fuel flow rate increase on the thermal performance of the combustor for different swirlers at the airflow rate of 2.4 slpm: (a) mean outer wall temperature and (b) emitter efficiency.

Table 3: Enhancement of emitter efficiency when compared with nonswirling flames (F0O0) at three fuel flow rates.

Swirler	Emitter efficiency enhancement (%)		
	$\dot{Q}_{CH_4}$ = 0.050 slpm	$\dot{Q}_{CH_4}$ = 0.100 slpm	$\dot{Q}_{CH_4}$ = 0.150 slpm
F30O0	18	9	13
F45O0	38	18	37
F0O30	353	126	43
F0O45	412	173	57

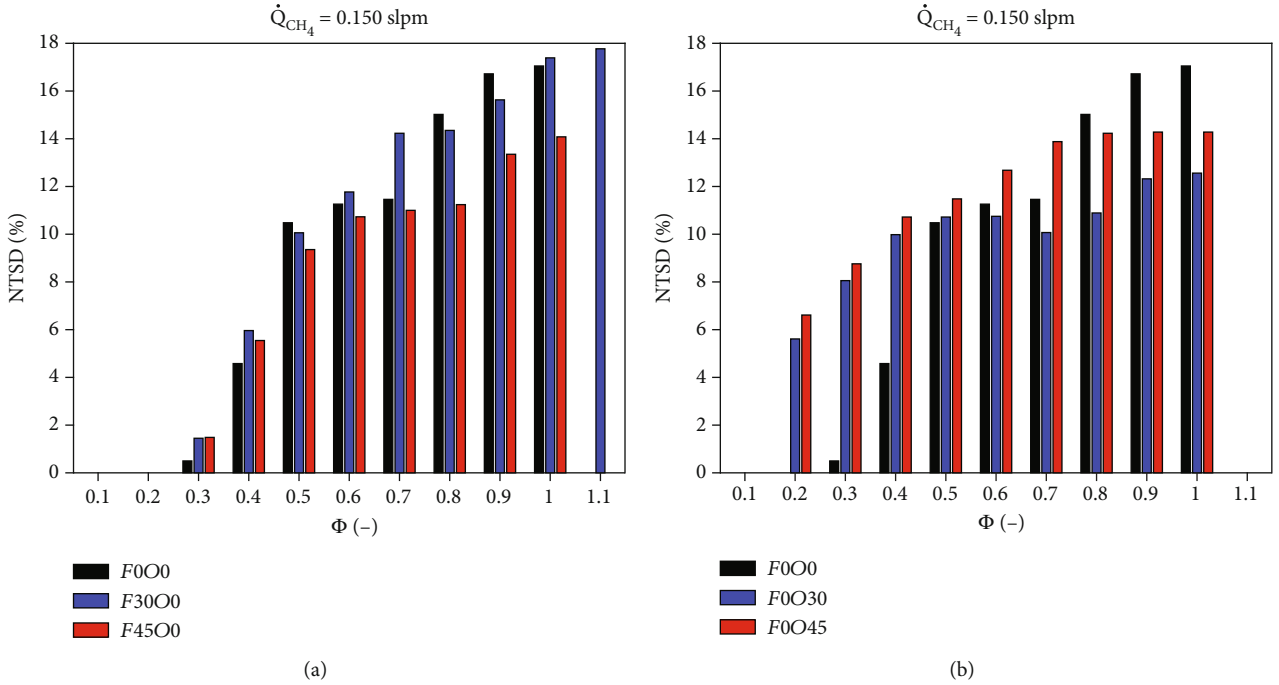

Figure 10: Effects of (a) fuel flow swirl and (b) airflow swirl on normalized temperature standard deviation as a function of equivalence ratio at the fuel flow rate of 0.150 slpm.

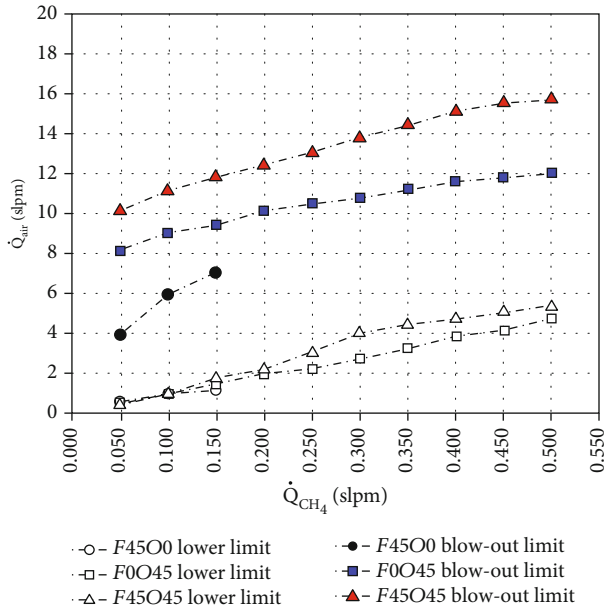

Figure 11: Combustor operational envelope for three swirlers of F45O0, F0O45, and F45O45.

17.77% and occurs for F30O0 at the equivalence ratio of 1.1. From Figure 10(b), it is observed that the NTSD of F0O30 is lower than that of F0O45, and for $\Phi \geq 0.5$, F0O30 has the lowest values of NTSD and the most uniform combustor wall temperature among three configurations of F0O0, F0O30, and F0O45. It is also observed that the NTSD of F0O0 takes the highest values for $\Phi \geq 0.8$. Furthermore, the NTSD of F0O45 remains almost constant and is not sensitive to the equivalence ratio for $\Phi \geq 0.7$.

Table 4: Enhancement of combustor operational envelope with F45O45 when compared with F45O0 and F0O45.

Swirler	Operational envelope enhancement (%)
Compared with F45O0	846
Compared with F0O45	27

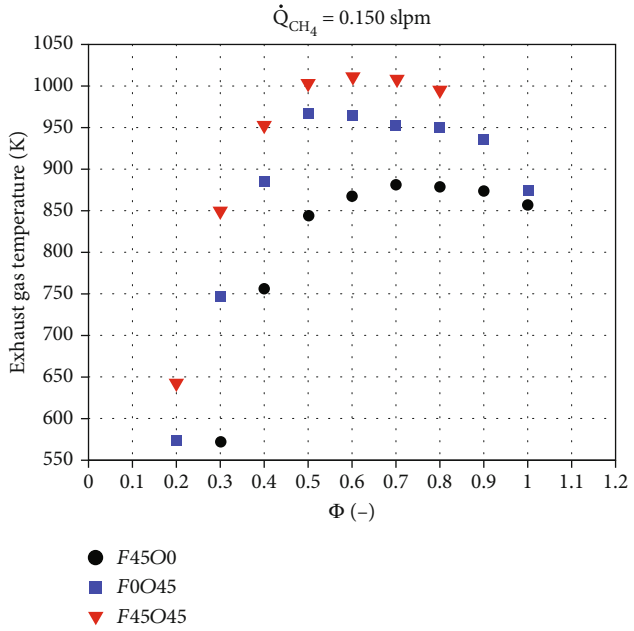

Figure 12: Exhaust gas temperature as a function of equivalence ratio at the fuel flow rate of 0.150 slpm for three swirlers of F45O0, F0O45, and F45O45.

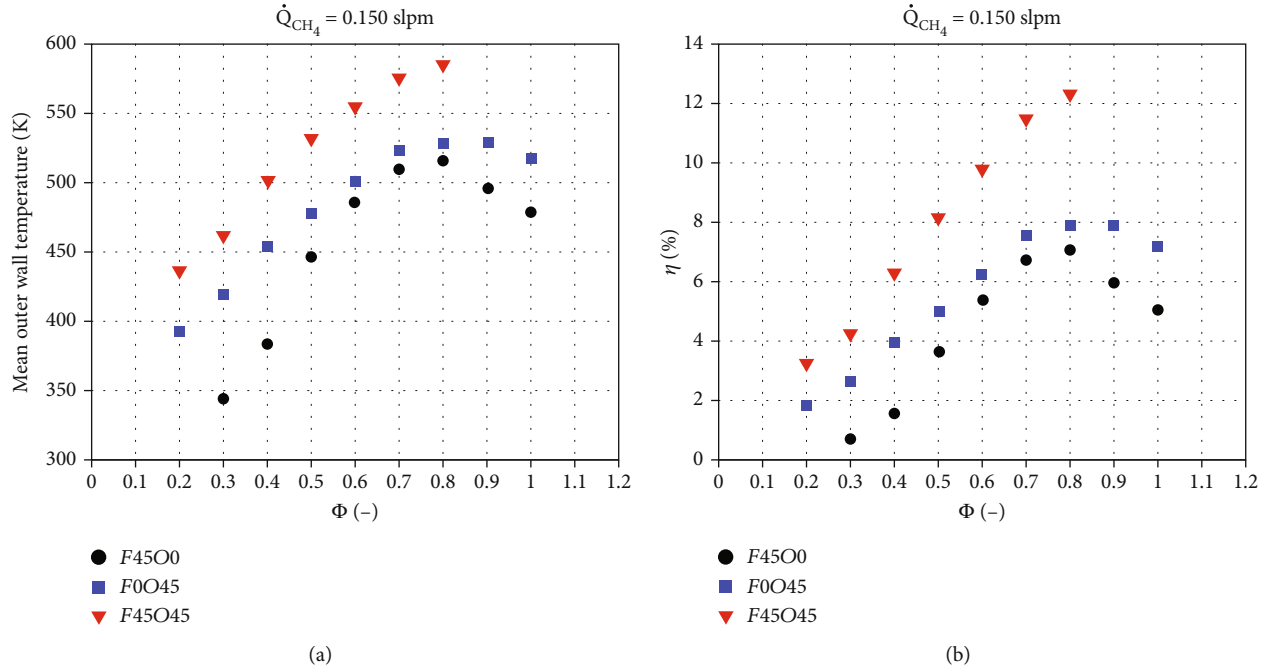

Figure 13: Variation of (a) mean outer wall temperature and (b) emitter efficiency with equivalence ratio at the fixed fuel flow rate of 0.150 slpm for three swirlers of F45O0, F0O45, and F45O45.

3.2. Simultaneous Swirling Flows of Fuel and Oxidizer. It was observed that adding a swirl to fuel flow or airflow enhances the operational envelope of the combustor. Besides, increasing the swirl number of fuel flow or airflow enhances the mean outer wall temperature and emitter efficiency of the combustor because of the enhancement of combustion efficiency and the amount of heat released at the same operating conditions. So, F45O0 (from the group including F0O0, F30O0, and F45O0) and F0O45 (from the group including F0O0, F0O30, and F0O45) have the highest combustor operational envelope, combustor mean outer wall temperature, and combustor emitter efficiency. Based on these outcomes, in this section, a swirler that takes advantage of simultaneous swirling flows of fuel and oxidizer (F45O45) is investigated, and its operational envelope and thermal performance are compared with two other swirlers, F45O0 and F0O45.

Figure 11 represents the combustor operational envelope of swirlers F45O0, F0O45, and simultaneous swirling flows of fuel and air (F45O45). This figure indicates that without a coairflow swirl, it was not possible to maintain the flame within the combustor at fuel flow rates greater than 0.150 slpm. This graph also shows how the blowout limit of the combustor increases significantly when a swirl is added to the coairflow. Furthermore, it is observed that simultaneous swirling flows of fuel and air (F45O45) enhance the blowout limit compared to solely airflow swirl. By comparing the lower limits related to F45O0, F0O45, and F45O45, it is observed that flame formation inside the combustor takes place at higher airflow rates for F45O45 compared with other swirlers. This can be attributed to the weak performance of F45O45 in fuel and air mixing at low airflow rates. However, the combustor operational envelope is the best for the F45O45 configuration. This enhancement is summarized in Table 4.

Figure 12 depicts the variation of exhaust gas temperature as a function of the equivalence ratio for the abovementioned swirlers. It is observed that as the equivalence ratio rises (the airflow rate falls), the temperature of the exhaust gas shows increasing-decreasing behavior. Additionally, it has been demonstrated that swirlers with coaxial airflow swirl (F0O45 and F45O45) result in higher exhaust gas temperatures compared with the swirler with fuel flow swirl (F45O0). Moreover, the exhaust gas temperature has the highest values in simultaneous swirling flows of fuel and air. This can be attributed to the completeness of the combustion due to better mixing and the higher amount of heat generated in the case of F45O45.

Figures 13(a) and 13(b) show the variation of mean outer wall temperature and emitter efficiency with the equivalence ratio at the fixed fuel flow rate of 0.150 slpm. The lower values of mean outer wall temperatures and emitter efficiencies at lower equivalence ratios (higher airflow rate) can be explained by lower combustion efficiency and flow residence time, which subsequently lead to a lower amount of heat generated and insufficient time for heat to be transferred to the combustor wall. It is observed that swirlers with coaxial airflow swirl (F0O45 and F45O45) result in higher mean outer wall temperature and emitter efficiency compared with the swirler with fuel flow swirl (F45O0). This can be attributed to the enhancement of combustion efficiency and the amount of heat released by utilizing airflow swirl at the same operating conditions. Besides, the mean outer wall temperature and emitter efficiency have the highest values in simultaneous swirling flows of fuel and air at the same operating conditions compared with other swirlers. That is because of the completeness of the combustion due to better mixing and the amount of heat generated in the

case of F45O45. It can also be attributed to the longest flow residence time related to F45O45, which provides more time for heat produced to be transferred to the combustor wall.

4. Conclusion

In this work, due to the well-known impact of swirling flows in flame stabilization, the effects of fuel flow and airflow swirl on the combustor operational envelope, flame blowout, and emission and thermal performances of a mesoscale combustor are studied. The obtained results can be useful in designing combustion-based thermophotovoltaic micropower generators. The main findings are summarized as follows:

(1) Swirl addition to fuel flow or coaxial airflow enhances the combustor operational envelope and the flame resistance against extinction (blowout). The operational envelope enhancement achieved for airflow swirl addition mode is more significant (≈798% for 45° vane angle for airflow) than that of for fuel flow swirl addition mode (≈30% for 45° vane angle for fuel stream) when compared with nonswirling flames. Hence, it can be concluded that airflow swirl is more favorable for flame stabilization when compared with fuel flow swirl. Furthermore, simultaneous swirling flows of fuel and air enhance the combustor operational envelope further (≈846% compared with F45O0 and ≈27% compared with F0O45)

(2) Combustion efficiency and the amount of heat released increase with a swirl addition to the fuel flow or the airflow, which consequently influences the exhaust gas temperature, mean outer wall temperature, and emitter efficiency. The mentioned parameters reveal an increasing-decreasing trend with an increment in the equivalence ratio where the methane flow rate is fixed. Furthermore, as the swirl strength of the fuel or airflows increases combustion efficiency, exhaust gas temperature, mean outer wall temperature, and emitter efficiency rise, too. Besides, the mean outer wall temperature and emitter efficiency of simultaneous swirling flows of fuel and air (F45O45) have the highest values compared with other swirlers. So, it can be concluded that the F45O45 swirler is the best choice for a combustion-based thermophotovoltaic power generation from the emitter efficiency point of view

(3) Increasing the fuel flow swirl number generally lessens the NTSD and consequently improves the combustor wall temperature uniformity, while for the airflow swirl case, a 30° vane angle swirler for airstream has lower NTSD than a 45° vane angle swirler. Besides, the 30° vane angle swirler for airflow reveals the lowest values of NTSD and the most wall temperature uniformity for $\Phi \geq 0.5$ among the three configurations (nonswirling flames, the 30° vane angle swirler, and the 45° vane angle swirler)

Nomenclature

$\dot{Q}_{CH_4}$: Methane volume flow rate (slpm)
$\dot{Q}_{air}$: Airflow rate (slpm)
Φ: Equivalence ratio (-)
S_n: Swirl number (-)
D_h: Swirler hub diameter (mm)
D_{sw}: Swirler tip diameter (mm)
θ: Swirler vane angle (°)
T_{amb}: Ambient temperature (°C)
P_{amb}: Ambient pressure (Pa)
RH: Ambient humidity (%)
T_{exh}: Exhaust gas temperature (K)
$T_{w,i}$: Wall temperature of element surface i (K)
$A_{w,i}$: Area of element surface i (m^2)
ε: Emissivity (-)
δ: Stephen-Boltzmann constant (5.67×10^{-8} W/(m^2-K))
$\dot{Q}_{rad}$: Radiation heat loss (W)
η: Emitter (radiation efficiency) (%)
T_{ave}: Mean combustor outer wall temperature (K)
$\dot{m}_{CH_4}$: Methane mass flow rate (kg/s)
LHV_{CH_4}: Lower heating value of methane (kJ/kg)
A: Combustor outer wall area (m^2).

Data Availability

All data used to support the findings of this study are included within the article.

Conflicts of Interest

The authors declare that they have no conflicts of interest.

Acknowledgments

The authors acknowledge the financial support from the Erasmus+ International Credit Mobility grant administered by Alianza 4 Universidades, Spain.

References

[1] M. B. Tulu, G. Li, D. B. Alemayehu, and M. Yi, "A free-standing, silent, micro/mesoscale combustion-powered thermoelectric generator based on natural convection cooling," *Journal of Heat Transfer*, vol. 144, no. 5, article 052601, 2022.

[2] G. N. Li, M. B. Yi, M. B. Tulu, Y. Q. Zheng, W. W. Guo, and Y. J. Tang, "Miniature self-powering and self-aspirating combustion-powered thermoelectric generator burning gas fuels for combined heat and power supply," *Journal of Power Sources*, vol. 506, article 230263, 2021.

[3] G. Li, Z. Zhu, Y. Zheng, W. Guo, Y. Tang, and C. Ye, "Experiments on a powerful, ultra-clean, and low-noise-level swirl-combustion-powered micro thermoelectric generator," *Energy*, vol. 263, article 125825, 2023.

[4] N. S. Kaisare and D. G. Vlachos, "A review on microcombustion: fundamentals, devices and applications," *Progress in Energy and Combustion Science*, vol. 38, no. 3, pp. 321–359, 2012.

[5] K. Maruta, "Micro and mesoscale combustion," *Proceedings of the Combustion Institute*, vol. 33, no. 1, pp. 125–150, 2011.

[6] Y. Ju and K. Maruta, "Microscale combustion: technology development and fundamental research," *Progress in Energy and Combustion Science*, vol. 37, no. 6, pp. 669–715, 2011.

[7] Y. Ju, C. Cadou, and K. Maruta, *Microscale Combustion and Power Generation*, Momentum Press, 2014.

[8] Y.-C. Chao, G.-B. Chen, C.-J. Hsu, T.-S. Leu, C.-Y. Wu, and T.-S. Cheng, "Operational characteristics of catalytic combustion in a platinum microtube," *Combustion Science and Technology*, vol. 176, no. 10, pp. 1755–1777, 2004.

[9] D. G. Norton, E. D. Wetzel, and D. G. Vlachos, "Fabrication of single-channel catalytic microburners: effect of confinement on the oxidation of hydrogen/air mixtures," *Industrial & Engineering Chemistry Research*, vol. 43, no. 16, pp. 4833–4840, 2004.

[10] G. Veser, "Experimental and theoretical investigation of H_2 oxidation in a high-temperature catalytic microreactor," *Chemical Engineering Science*, vol. 56, no. 4, pp. 1265–1273, 2001.

[11] V. Shirsat and A. K. Gupta, "Performance characteristics of methanol and kerosene fuelled meso-scale heat-recirculating combustors," *Applied Energy*, vol. 88, no. 12, pp. 5069–5082, 2011.

[12] A. Tang, T. Cai, J. Deng, Y. Xu, and J. Pan, "Experimental investigation on combustion characteristics of premixed propane/air in a micro-planar heat recirculation combustor," *Energy Conversion and Management*, vol. 152, pp. 65–71, 2017.

[13] M. Shantanu, V. Mahendra Reddy, and S. Karmakar, "Experimental and numerical studies on heat recirculated high intensity meso-scale combustor for mini gas turbine applications," *Energy Conversion and Management*, vol. 176, pp. 324–333, 2018.

[14] M.-h. Wu, Y. Wang, V. Yang, and R. A. Yetter, "Combustion in meso-scale vortex chambers," *Proceedings of the Combustion Institute*, vol. 31, no. 2, pp. 3235–3242, 2007.

[15] S. E. Hosseini, E. Owens, J. Krohn, and J. Leylek, "Experimental investigation into the effects of thermal recuperation on the combustion characteristics of a non-premixed meso-scale vortex combustor," *Energies*, vol. 11, no. 12, p. 3390, 2018.

[16] D. Shimokuri, Y. Honda, and S. Ishizuka, "Flame propagation in a vortex flow within small-diameter tubes," *Proceedings of the Combustion Institute*, vol. 33, no. 2, pp. 3251–3258, 2011.

[17] D. Shimokuri, Y. Taomoto, and R. Matsumoto, "Development of a powerful miniature power system with a meso-scale vortex combustor," *Proceedings of the Combustion Institute*, vol. 36, no. 3, pp. 4253–4260, 2017.

[18] Y. Lei, W. Chen, and J. Lei, "Combustion and direct energy conversion inside a micro-combustor," *Applied Thermal Engineering.*, vol. 100, pp. 348–355, 2016.

[19] Y. Gan, X. Chen, Y. Tong, X. Zhang, and Y. Zhang, "Thermal performance of a meso-scale combustor with electrospray technique using liquid ethanol as fuel," *Applied Thermal Engineering*, vol. 128, pp. 274–281, 2018.

[20] D. Shimokuri, T. Hara, and R. Matsumoto, "Development of a small-scale power system with meso-scale vortex combustor and thermo-electric device," *Journal of Micromechanics and Microengineering*, vol. 25, no. 10, article 104004, 2015.

[21] X. Yang, L. Zhao, Z. He, S. Dong, and H. Tan, "Comparative study of combustion and thermal performance in a swirling micro combustor under premixed and non-premixed modes," *Applied Thermal Engineering*, vol. 160, article 114110, 2019.

[22] A. H. Epstein, S. D. Senturia, G. Anathasuresh et al., "Power MEMS and microengines," in *Proceedings of International Solid State Sensors and Actuators Conference (Transducers '97)*, Chicago, IL, USA, June 1997.

[23] A. Epstein, "Millimeter-scale, micro-electro-mechanical systems gas turbine engines," *Journal of Engineering for Gas Turbines and Power*, vol. 126, no. 2, pp. 205–226, 2004.

[24] K. Fu, A. J. Knobloch, F. C. Martinez et al., "Design and experimental results of small-scale rotary engines," in *ASME 2001 International Mechanical Engineering Congress and Exposition*, New York, USA, November 2001.

[25] W. Dahm, J. Mijit, R. Mayor et al., "Micro internal combustion swing engine (MICSE) for portable power generation systems," in *40th AIAA Aerospace Sciences Meeting & Exhibit*, 2002.

[26] M.-H. Wu and P.-S. Lin, "Design, fabrication and characterization of a low-temperature co-fired ceramic gaseous bipropellant microthruster," *Journal of Micromechanics and Microengineering*, vol. 20, no. 8, article 085026, 2010.

[27] T. Liu, F. Bai, Z. Zhao, Y. Lin, Q. Du, and Z. Peng, "Large eddy simulation analysis on confined swirling flows in a gas turbine swirl burner," *Energies*, vol. 10, no. 12, p. 2081, 2017.

[28] J. O'Connor and T. Lieuwen, "Recirculation zone dynamics of a transversely excited swirl flow and flame," *Physics of Fluids*, vol. 24, no. 7, article 075107, 2012.

[29] D. Feikema, R.-H. Chen, and J. F. Driscoll, "Enhancement of flame blowout limits by the use of swirl," *Combustion and Flame*, vol. 80, no. 2, pp. 183–195, 1990.

[30] M. Zaitri, M. Bouchetara, A. Bouziane, and A. Alami, "Effect of CH_4-H_2 mixture on the combustion characteristics in a stabilized swirl burner," *International Journal of Energy Research*, vol. 46, no. 3, pp. 2923–2933, 2022.

[31] C. Tao, B. Liu, Y. Dou, Y. Qian, Y. Zhang, and S. Meng, "The experimental study of flame height and lift-off height of propane diffusion flames diluted by carbon dioxide," *Fuel*, vol. 290, article 119958, 2021.

[32] W. Gao, N. Liu, Y. Jiao et al., "Flame length of non-buoyant turbulent slot flame," *Proceedings of the Combustion Institute*, vol. 37, no. 3, pp. 3843–3850, 2019.

[33] Z. Zhou, G. Chen, C. Zhou, K. Hu, and Q. Zhang, "Experimental study on determination of flame height and lift-off distance of rectangular source fuel jet fires," *Applied Thermal Engineering*, vol. 152, pp. 430–436, 2019.

[34] Z. Xi, Z. Fu, X. Hu, S. W. Sabir, and Y. Jiang, "An experimental investigation on the NO and CO emission characteristics of a swirl convergent-divergent nozzle at elevated pressure," *Energies*, vol. 11, no. 6, p. 1410, 2018.

[35] S. McAllister, J. Y. Chen, and A. C. Fernandez-Pello, *Fundamentals of Combustion Processes*, Springer, New York, 2011.

[36] D. C. Kyritsis, S. Roychoudhury, C. S. McEnally, L. D. Pfefferle, and A. Gomez, "Mesoscale combustion: a first step towards liquid fueled batteries," *Experimental Thermal and Fluid Science*, vol. 28, no. 7, pp. 763–770, 2004.